Advanced International Journal for Research (AIJFR)
E-ISSN: 3048-7641 ● Website: www.aijfr.com ● Email: editor@aijfr.com

Numerical Simulation of Hypersonic Inflatable Aerodynamic Decelerators

Arun Prathap[1], Sai K. Ullal[2], Rishab M. Chitgopekar[3], Raunak G. Mahenderkar[4], Deepanshu K. Punjabi[5], Jayahar Sivasubramanian[6]

[1,2,3,4,5,6] Department of Aerospace and Automotive Engineering, M. S. Ramaiah University of Applied Sciences, Bangalore, India

Abstract

This paper uses CFD simulations to examine and assess a Hypersonic Inflatable Aerodynamic Decelerator (HIAD) to create technologies for landing big payloads on planets with thin atmospheres. Because it includes extreme physical conditions, atmospheric entry is one of the most challenging phases of most space missions. These severe physical conditions need a comprehensive grasp of hypersonic flow, which is the flow regime in which they occur. The flexible thermal protection cover of the Hypersonic Inflatable Aerodynamic Decelerator deforms during the re-entry phase. As a result, an in-depth investigation into the subject is required to analyze heat transfers and pressure distributions on the body's surface in order to prevent structural failures. This study used the SU2 open domain CFD software to do the necessary CFD simulations to evaluate the flow mechanics over the body. The GMSH tool was used to build the high-quality grids required for this project. SU2's advanced NEMO solver and the Mutation++ library may be used to simulate and explore non-equilibrium flows, providing a thorough and in-depth understanding of the effects of hypersonic flows on the body during the planetary entry phase. This study has the potential to be extended to 3D HIAD geometries, allowing for a more complete knowledge of high-speed flows through atmospheric entry modules at varied angles of attack. This research focuses on achieving the best results for 2D geometries and investigates heat transport on the body's surface, validating experimental results as well as comparing results from conventional and non-equilibrium flow solvers.

Keywords: CFD, SU2, HIAD, Hypersonic Flight, Aerodynamic Decelerator.

1. Introduction

The HIAD is an inflatable body that is used to slow the body when it enters the atmosphere at high hypersonic speeds. Entry capsule drag limits payload mass on Mars and other destinations with thin atmospheres [1]. Traditional re-entry modules have a small aeroshell area and are not well suited for low density atmospheres. The HIAD, on the other hand, has a larger aeroshell area and is better suited for low density atmospheres. Before coming in contact with the outer environment, the HIAD aeroshell is stored inside the body and then deployed to a wider diameter. Because carrying a full re-entry module would take up a lot of room, this approach of deploying flexible aeroshells in a compact manner saves a lot of space for the payload. This is the point at which the aeroshell is launched. The HIAD offers a large surface area for drag production when deployed and inflated, resulting in a lower ballistic coefficient than a rigid aeroshell of similar surface area. Because much of the deceleration for the HIAD occurs at high altitudes

where the environment is not as thick as it is for standard re-entry modules, the peak heat flux of the HIAD is substantially lower [2]. In contrast to standard re-entry modules, which require a dense environment for deceleration, this one does not. The surface of the HIAD begins to distort under strong aerodynamic stresses during re-entry, a phenomenon known as scalloping. For varying degrees of aerodynamic stress, the degree of scalloping varies [3,4].

2. Literature Review and Objective

Entry, descent, and landing (EDL) on planets like Mars is problematic because the atmosphere is too thin to provide substantial deceleration yet thick enough to generate significant heating on re-entry. One way for landing heavy payloads on such worlds is to use a Hypersonic Inflatable Aerodynamic Decelerator. HIADs are comprised of lightweight, flexible materials that may be folded into a smaller volume and inflated before atmospheric impact in the rocket payload fairing. It is one of the only ways to drop a significant quantity payload on such planets with a thin atmosphere due to its ability to be stowed in current launch vehicles. However, various research and testing must be carried out in order to build an HIAD with a technical readiness of at least level 8. It is evident that these experiments cannot be carried out directly in the Martian environment. As a result, an HIAD is first built for Earth re-entry, and the EDL is carefully tested and analyzed in order to show and make the technology dependable.

A. Gas models

The perfect gas model assumes that the gas molecules are indistinguishable, tiny, and hard spheres, that there are no energy losses in motion or during molecule collisions, and that the average distance between molecules is substantially greater than the size of the molecules. The molecules of the gas, on the other hand, dissociate and ionize at high temperatures. The gas's specific heat is a function of its pressure and temperature. As a result, ideal gases cannot be employed since the gas cannot be considered to be calorically perfect. Because of molecular collisions, vibrational and chemical changes occur at high temperatures. However, for the modifications to occur, a significant number of collisions must occur, which takes time. In equilibrium systems, it is assumed that the gas has adequate time to collide and that the system's attributes are constant at a set pressure and temperature. The vibrational and chemical characteristics of non-equilibrium systems vary following a rapid change in pressure and temperature. Collisions between molecules are required for the system's elements to achieve this new equilibrium state, and this takes time. The non-equilibrium flow area exists between the time it takes for the system to reach its new equilibrium phase and the time it takes for the system to reach its new equilibrium phase.

B. High-altitude and high-speed flow features

The environment behind a typical shock in front of the entrance module will be substantially different from the atmosphere before the shock in the higher levels of the atmosphere, when atmospheric entry speeds approach Mach 20. Due to a decrease in sound velocity and an increase in air density, the peak surface heat flux increases as altitude decreases in free stream circumstances. The normal shock strength increases as the free stream velocity increases, according to gas dynamics [5,6].

At these high altitudes, hypersonic fluxes including predominantly nitrogen and oxygen cause dissociation and ionization of the molecules over a specific temperature. This causes non-equilibrium flow zones around the re-entry body, which alters flow characteristics. The ionized species form a plasma layer around

the body, which is responsible for the re-entry communication blackout. The novel species created by ionization will need the development of a new gas model that accounts for vibrational temperatures as well as forward and backward chemical reaction rates.

C. Dissociation effects high-temperature gas dynamics

When a gas's internal energy cannot be described by a single temperature during high-speed flows, thermal nonequilibrium occurs, whereas chemical nonequilibrium happens when its chemical state does not match chemical equilibrium criteria. Thermal and chemical non-equilibrium zones emerge as a result. This is because as the gas travels over the bow shock wave, much of its kinetic energy is transformed to random translational motion. Collisions transform the translational energy to rotational, vibrational, electronic, and chemical energy. This energy transfer necessitates a certain number of collisions, during which time the gas moves to a new location, perhaps altering temperature and density. The energy carried by polyatomic molecules in a gas-phase species is divided by translational, rotational, vibrational, and electronic degrees of freedom. The energy of each mode is quantized, and the allowable energy levels are specified by the eigenstates of the time-independent Schrödinger equation [5].

SU2-NEMO uses a two-temperature model to track the translational–rotational energy modes and vibrational–electronic energy modes separately to account for differences in the number of collisions necessary to establish equilibrium. The translational and rotational energy modes, as well as the vibrational and electronic modes, are thought to be in balance in this two-temperature model, however the two are not always in equilibrium.

Total energy and vibrational–electronic energy per unit volume in SU2 are expressed as:

$$\rho e = \sum_s \rho_s \left(e_s^{tr} + e_s^{rot} + e_s^{vib} + e_s^{el} + e_s^{\circ} + \frac{1}{2}\mathbf{u}^T\mathbf{u} \right) \tag{1}$$

And,

$$\rho e^{ve} = \sum_s \rho_s \left(e_s^{vib} + e_s^{el} \right) \tag{2}$$

Where,

$$e_s^{vib} = \begin{cases} \frac{R}{M_s} \frac{\theta_s^{vib}}{exp\left(\theta_s^{vib}/T^{ve}\right)-1} & \text{for polyatomic species,} \\ 0 & \text{for monatomic species and electrons,} \end{cases}$$

$$e_s^{el} = \begin{cases} \frac{R}{M_s} \frac{\sum_{i=1}^{\infty} g_{i,s}\theta_{i,s}^{el} exp\left(-\theta_{i,s}^{el}/T_{ve}\right)}{\sum_{i=0}^{\infty} g_{i,s} exp\left(-\theta_{i,s}^{el}/T_{ve}\right)} & \text{for polyatomic and monatomic species,} \\ \frac{3}{2}\frac{R}{M_s}T^{ve} & \text{for electrons,} \end{cases}$$

D. Governing equations

The Navier-Stokes equations and the SU2-NEMO governing equations were utilized in the simulation, hence additional equations that may be employed are not given. SU2 solves the compressible Navier-Stokes equations in differential form, which are written as:

$$\mathcal{R}(U) = \frac{\partial U}{\partial t} + \nabla \cdot \bar{F}^c(U) - \nabla \cdot \bar{F}^v(U, \nabla U) - S = 0 \tag{3}$$

where the working variables are conservative variables and are provided by:

$$U = \{p, pi, pEy\}"$$

The convective and viscous fluxes are: S is a general source term, and the convective and viscous fluxes are:

$$\bar{F}^c = \begin{Bmatrix} \rho\bar{v} \\ \rho\bar{v} \otimes \bar{v} + \bar{\bar{I}}p \\ \rho E\bar{v} + p\bar{v} \end{Bmatrix}$$

$$\bar{F}^v = \begin{Bmatrix} \cdot \\ \bar{\bar{\tau}} \\ \bar{\bar{\tau}} \cdot \bar{v} + \kappa\nabla T \end{Bmatrix} \tag{4}$$

The Navier–Stokes equations are extended for reacting flows in thermochemical nonequilibrium to simulate continuum hypersonic flows in SU2-NEMO. The following are a set of connected nonlinear partial differential equations in conservation form:

$$\mathrm{R}(\mathrm{U}, \nabla \mathrm{U}) = \frac{\partial \mathrm{U}}{\partial t} + \nabla \cdot \mathrm{F}^c(\mathrm{U}) - \nabla \cdot \mathrm{F}^v(\mathrm{U}, \nabla \mathrm{U}) - \mathrm{Q}(\mathrm{U}) = 0 \tag{5}$$

For a number of species ns, the conservative variables, convective flux, viscous flux, and source terms are expressed in standard notation by:

$$\mathbf{U} = \begin{Bmatrix} \rho_1 \\ \vdots \\ \rho_{n_s} \\ \rho\mathbf{u} \\ \rho e \\ \rho e^{ve} \end{Bmatrix}, \mathbf{F}^c = \begin{Bmatrix} \rho_1\mathbf{u} \\ \vdots \\ \rho_{n_s}\mathbf{u} \\ \rho\mathbf{u}\mathbf{u}^T + P\not{\mathcal{I}} \\ \rho h\mathbf{u} \\ \rho e^{ve}\mathbf{u} \end{Bmatrix}, \mathbf{F}^v = \begin{Bmatrix} -\mathbf{J}_1 \\ \vdots \\ -\mathbf{J}_{n_s} \\ \sigma \\ \mathbf{u}^T\sigma - \sum_k \mathbf{q}^k - \sum_s \mathbf{J}_s h_s \\ -\mathbf{q}^{ve} - \sum_s \mathbf{J}_s e^{ve} \end{Bmatrix}, \mathbf{Q} = \begin{Bmatrix} \dot{\omega}_1 \\ \vdots \\ \dot{\omega}_{n_s} \\ \mathbf{0} \\ 0 \\ \dot{\Theta}^{tr:ve} + \sum_s \dot{\omega}_s e_s^{ve} \end{Bmatrix}, \tag{6}$$

E. Limitations and assumptions

Because the software being used is SU2, it is assumed that the continuum for the flow is still valid in the event when the re-entry module is high in the atmosphere and the Knudsen number is very high and continuum flow is no longer valid, and the flow must be considered rarefied. The best heat flux and temperature estimates would come from a DSMC combined with a non-equilibrium flow model performed on a very fine grid with over 10 million cells. However, because a supercomputer will be required, this is currently outside the scope of this paper. Finally, the simulations presented are confined to two-dimensional simulations at zero angle of attack due to computing constraints.

3. Methodology

For the purpose of running both equilibrium and nonequilibrium simulations, SU2 was used. Stanford University Unstructured is an open-source finite element or finite volume CFD solver. It was written in the C++ programming language and incorporates Python scripts that automate a variety of tasks and improve usability. The SU2-NEMO solver may be used to tackle non-equilibrium flow problems. With Mutation++, you may simulate a wide range of gas compositions. This library allows us to simulate non-equilibrium flows twice as fast as SU2's basic non-equilibrium resources. Therefore, It was frequently used in non-equilibrium flow simulations.

A. Problem statement

Two solvers were utilized in the CFD simulations on the HIAD to run a simulation for chemically non-reacting flow and a simulation for chemically reacting non-equilibrium flow. For the former, RANS equations were utilized, whereas for the latter, SU2's NEMO-solver was used. To simulate the initial atmospheric entry phase at high altitude circumstances, a Mach number of 26.7 is chosen. There are some common solver parameters, however SU2 NEMO requires certain unique settings to conduct the simulation. With the identical initial conditions, a Mach case of 6 is also explored to confirm experimental evidence from [9].

B. Geometry and Design

The HIAD has a heat protection layer and a malleable surface. These deformations arise as a result of the aeroshell's inflated nature, which necessitates a flexible surface. These deformations, on the other hand, can be employed to the system's benefit. Scalloping occurs when the surface deforms due to flight pressure stresses. This scalloping may be felt during the aeroshell's flight and descent, and it can add to the body's drag. Because performing non-rigid body simulations is difficult and beyond the scope of this research, simulations are instead carried out over multiple geometries of rigid geometries at various levels of scalloping, as is done in previous non-rigid body simulations. The scalloping angle, which is the angle between two consecutive tubes (toroid) within the inflated aeroshell, defines and recognizes the stages of scalloping. The CAD's geometry is specified below.

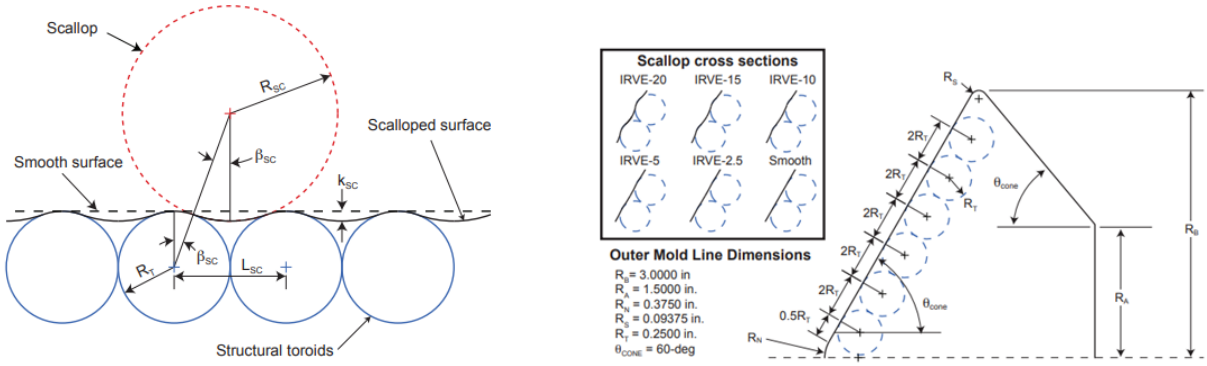

Figure 1 : Parametric scallop details and OML dimensions

Rigid body simulations aren't possible on HIAD directly as it has a constantly changing structure. To address this issue, multiple 2D meshes were created at various phases of body distortion. The stages are designated for the several levels of scalloping: 0, 5, 10, and 20.

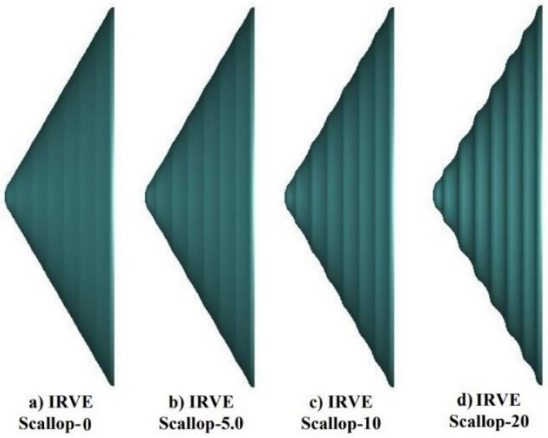

Figure 2 : Stages of scalloping [1]

C. Computational grid

The geometry was modelled into an unstructured mesh with a structured inflation layer using GMSH, which is an open-source software capable of generating meshes for SU2. The structured inflation layer was done to capture the boundary layer effects accurately, resulting in better surface data. The meshes used are depicted below:

1. **HIAD Scallop 0: Number of Cells - 591,828**

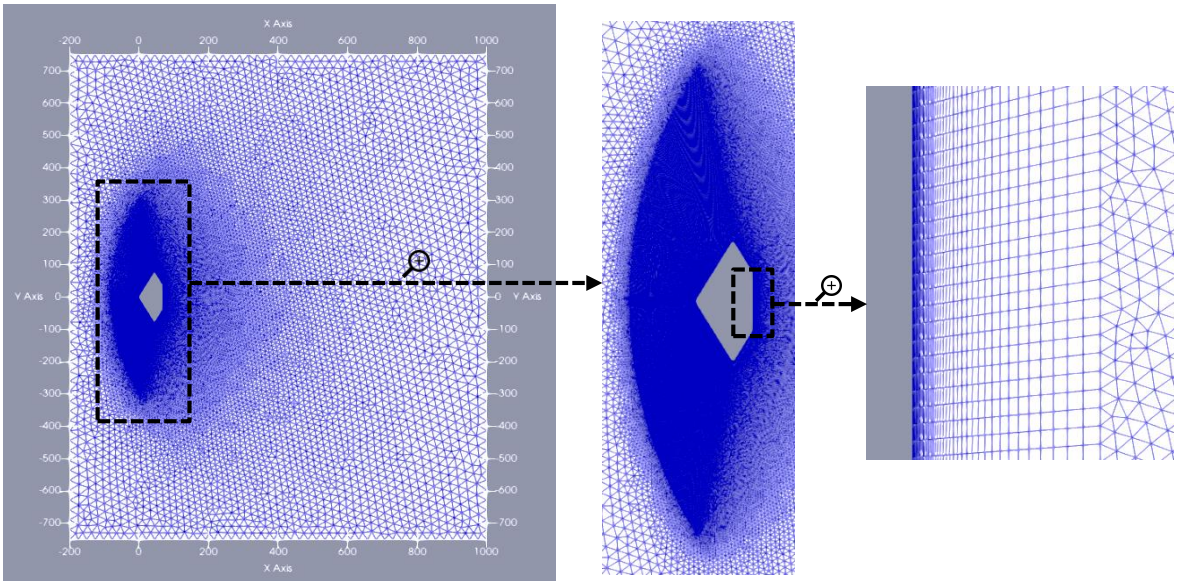

Figure 3 : Computational grid for zero scallop ranging from the whole domain on the left followed by shock refinement region and inflation layer at the end.

2. **HIAD Scallop 5: Number of Cells – 543,857**

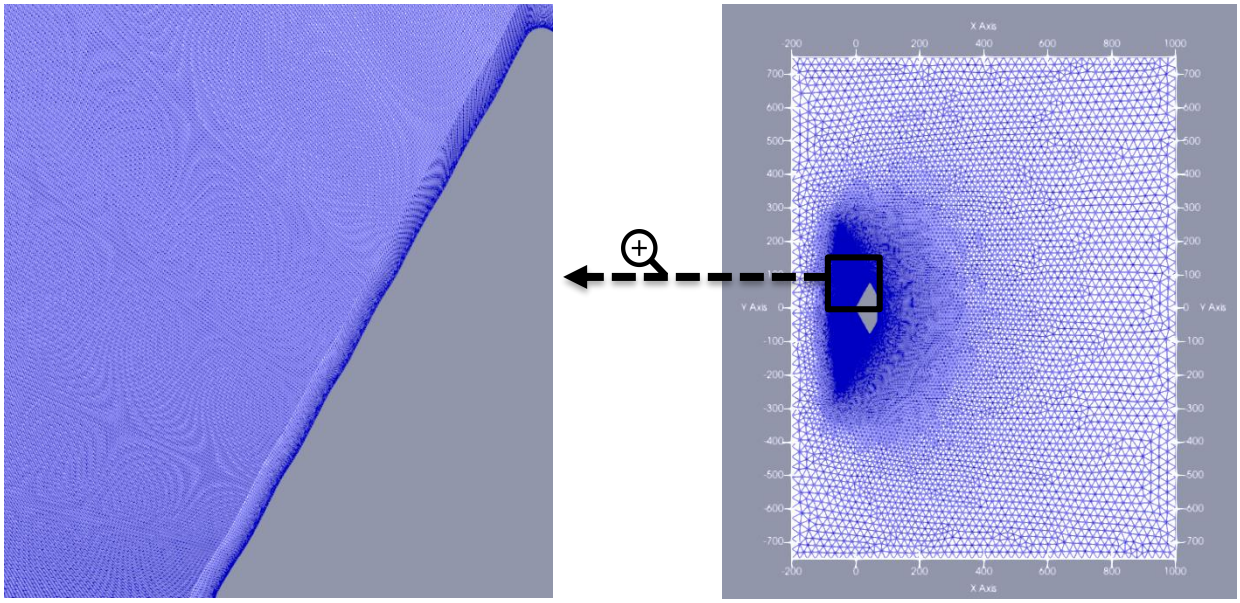

Figure 4 : Computational grid for scallop 5 geometry with zoomed inflation layer on the left and whole domain on the right

3. HIAD Scallop 10: Number of Cells – 542,243

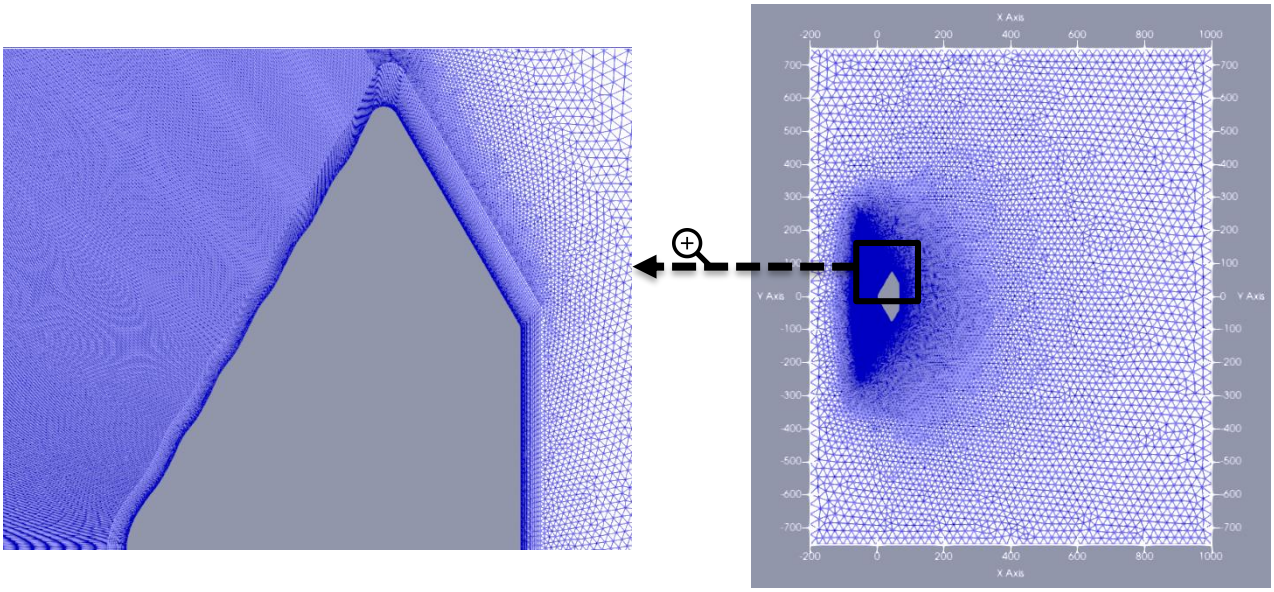

Figure 5 : Computational grid for scallop 10 with magnified image on the left and whole domain on the right

4. HIAD Scallop 20: Number of cells - 542,773

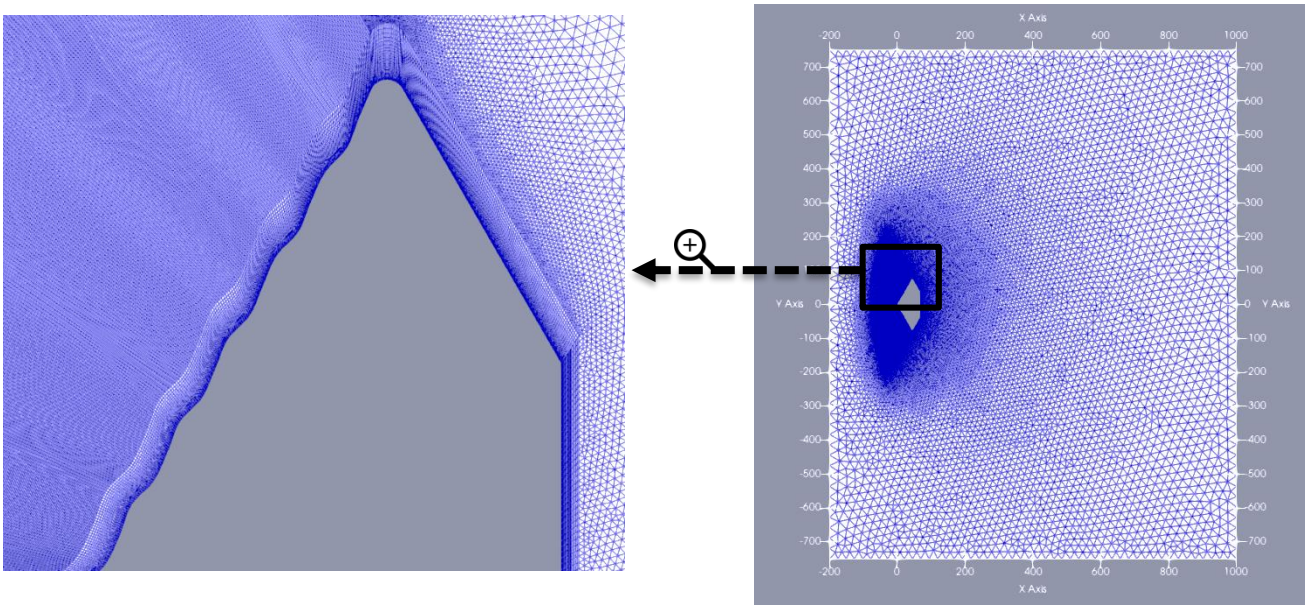

Figure 6 : Computational grid for scallop 20 geometry with magnified image on the left and whole domain on the right

D. Initial and boundary conditions

Table 1 : Important initial flow conditions and solver settings

Flow case	Chemically non-reacting flow	Chemically reacting non-equilibrium flow
Reynolds number	10E8	10E5
Mach number	26.7	
Freestream pressure	10 Pa	
Gas model	Ideal gas	Air_5 Mutation++
Freestream temperature	263K	195K
Knudsen number	0.03	
Governing equations	Reynolds Average Navier-Stokes (RANS)	NEMO Navier-Stokes equations
Turbulence model	Spalart-Allmaras	

It should be noted that the Air 5 Mutation++ gas model takes into consideration the gas's ionized species, and as a result, the temperature has been set lower than in standard gas models.

4. Results and Discussion

Due to the high-velocity re-entry, we know that a powerful shock wave occurs in front of the body. The translational temperature of the shock wave is also known to rise, generating a high-temperature zone. At higher altitudes, chemical processes in the shock layer occur at a slower pace, causing the translational temperature to rise. There is a low frequency of collisions between molecules due to the low density of the environment. The ideal gas model cannot predict precise temperature changes since it only considers energy transfers and heating as a result of molecular vibrations, as demonstrated in the temperature contours in the section below. As a result, the temperatures are overestimated, and the greater temperatures behind the body simply serve to corroborate this. We may argue that the conclusion is similar to that of the non-equilibrium model, but in the aftermath, we can observe a region forming without the inflated numbers. Because of the low pressure and very high temperatures behind the shock, the simulation is done at a very high altitude, typically between 80 and 100 kilometers. At these altitudes, collision frequency is minimal. Temperatures at this altitude are extremely high, reaching over 25,000K at a height of 100 kilometers [8].

The section focuses on the scalloping scenarios since these are RANS circumstances that expose the HIAD to the highest thermal shocks and structural deformations, followed by the pressure data for the various stages of the HIAD, after which the RANS case's translational temperatures are compared to the NEMO case's translational temperatures.

A. RANS results

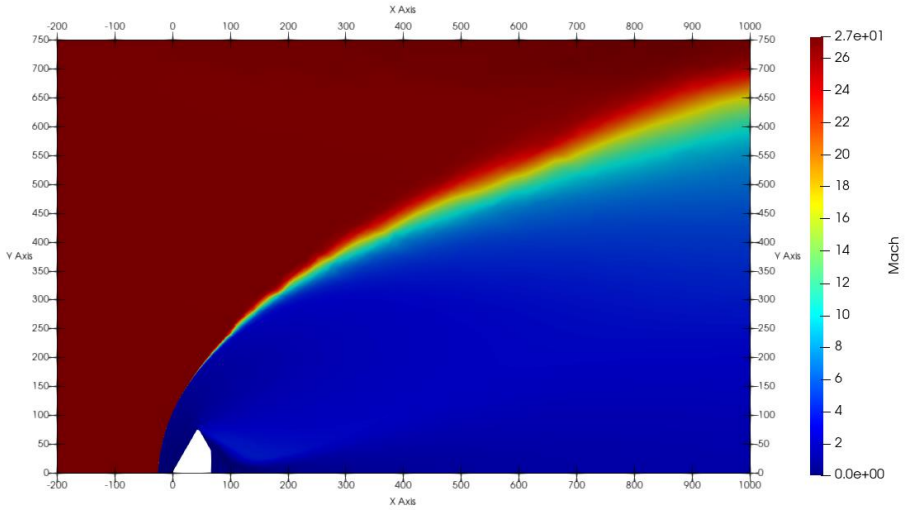

Figure 7 : HIAD-0 Mach contour

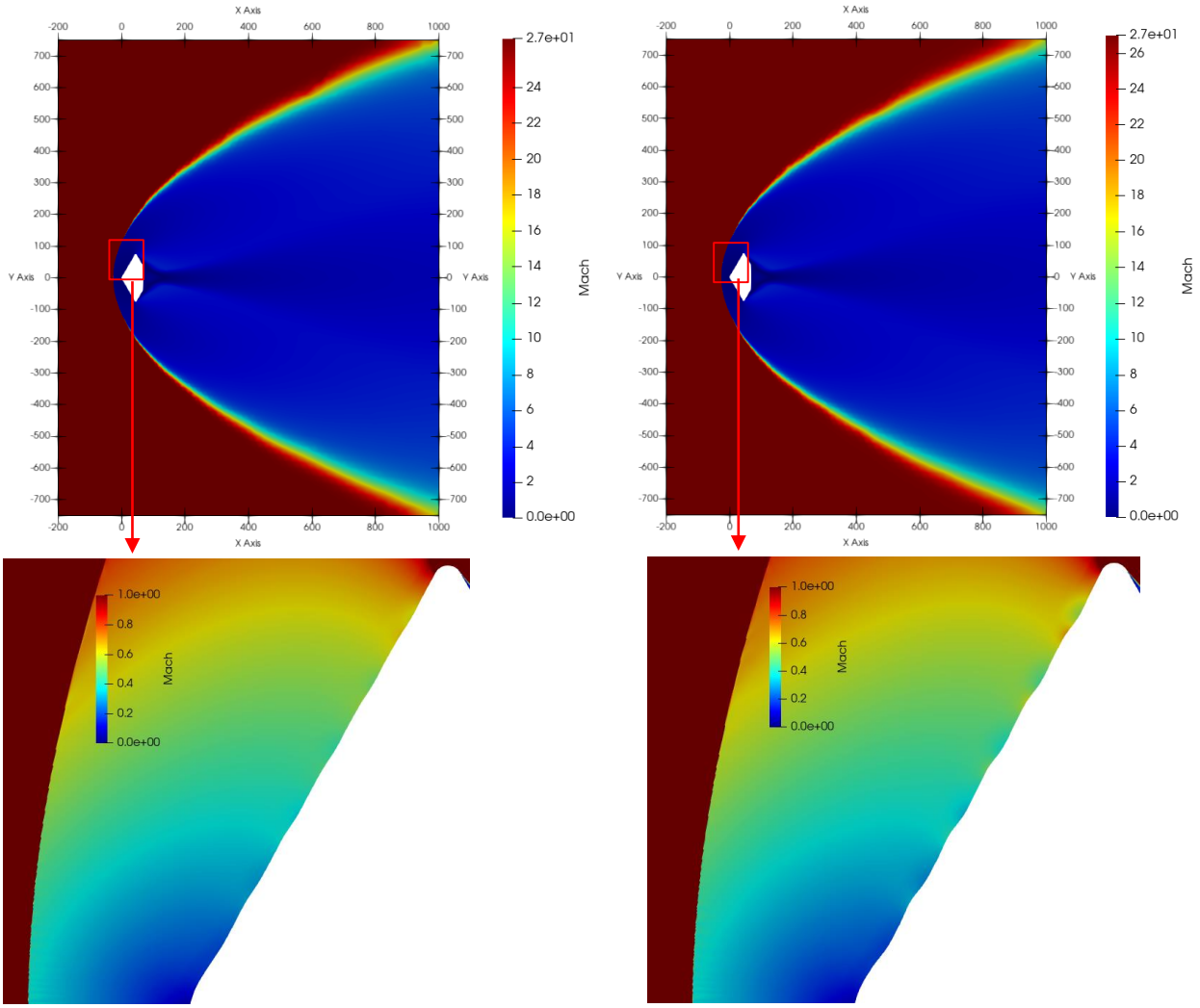

Figure 8 : Depicts the HIAD-5 and HIAD-10 scalloping stage with the zoomed-in image of the scallops

Figure 8 shows that scalloping has begun, and if we look closely, we can see that there are abrupt drops in Mach number on the tops of the scallops, followed by regions of much slower flow in the scallop pockets. This occurs as a result of the creation of oblique shock waves (see Figure 7), which is a common occurrence when oblique shocks occur in the flow. The shock lines are not visible since this is a RANS simulation rather than an LES (Large Eddy Simulation). The strength of the shocks on the scallops grew as the scalloping progressed due to the increased flow deflection angle. As a result, there will be a lot of local heating in the cavities and protuberances, which raises the possibility that the thermal pressures at the irregularity regions will be enough to trigger local heatshield structural failure (see Figure 9 and 10). The heating analysis in the next section elucidates this issue with localized heating.

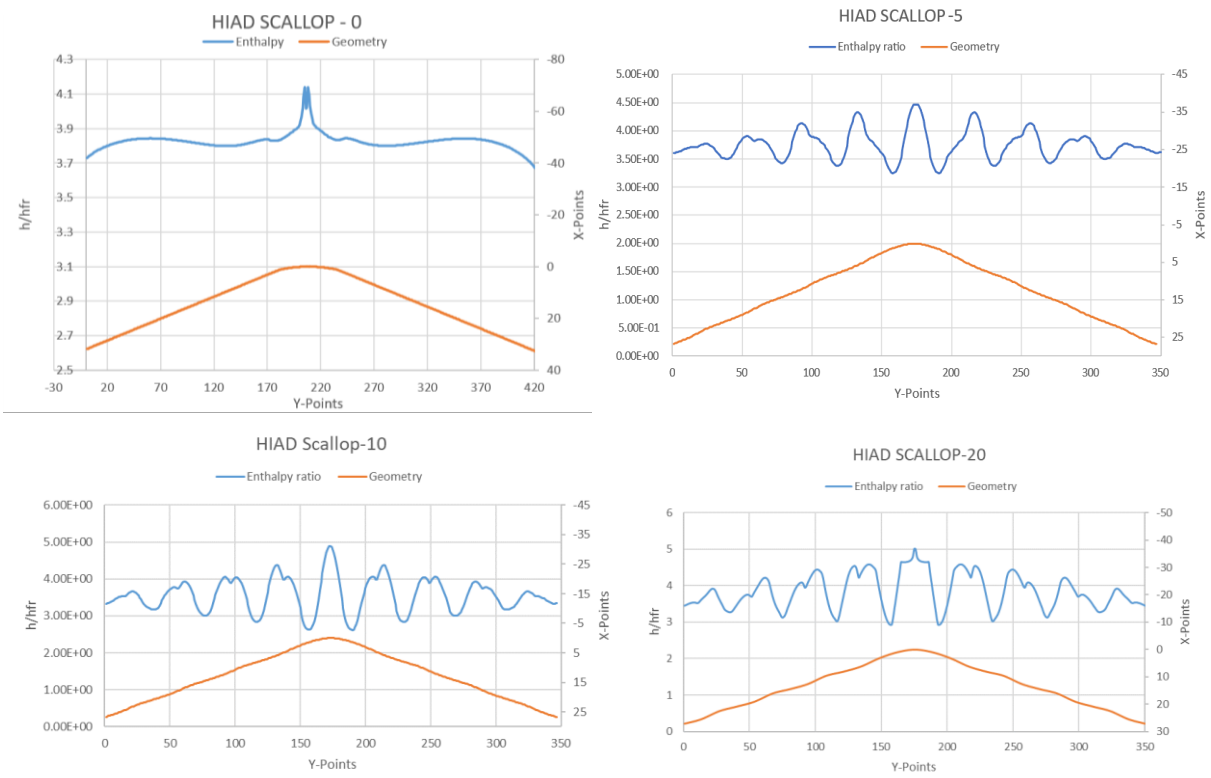

Figure 9 h/hfr ratio Vs the HIAD geometry for all degrees scalloping

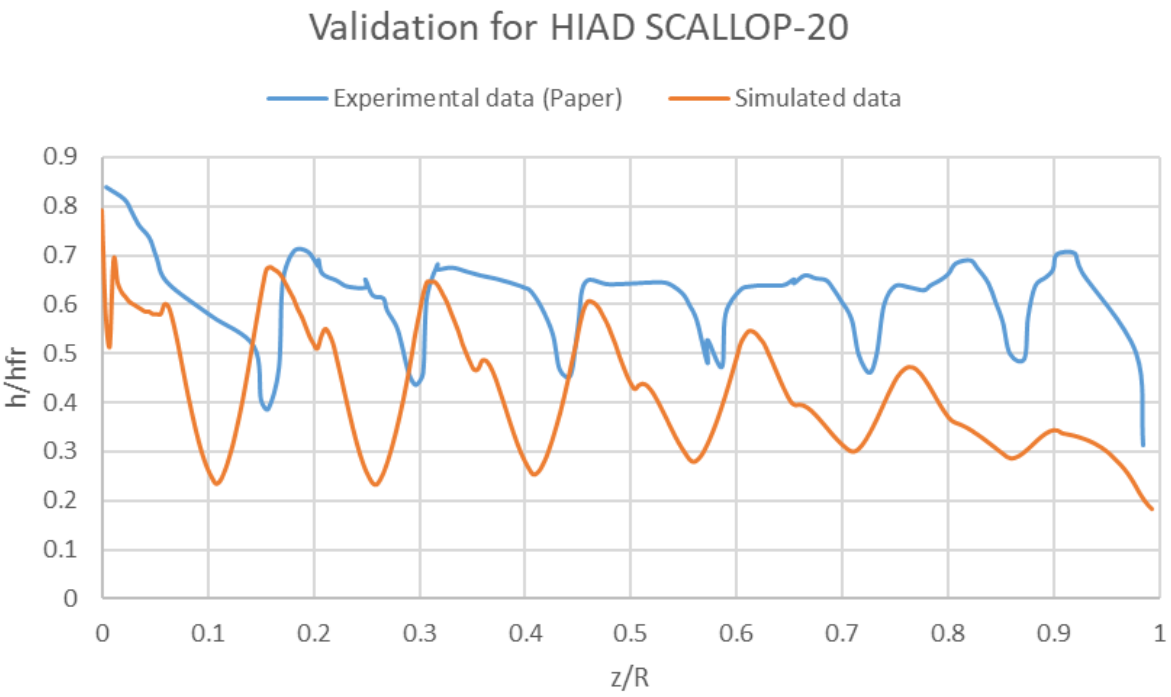

Figure 10 : Comparison of experimental heat-transfer data with the heat-transfer data obtained from the simulation.

B. NEMO results

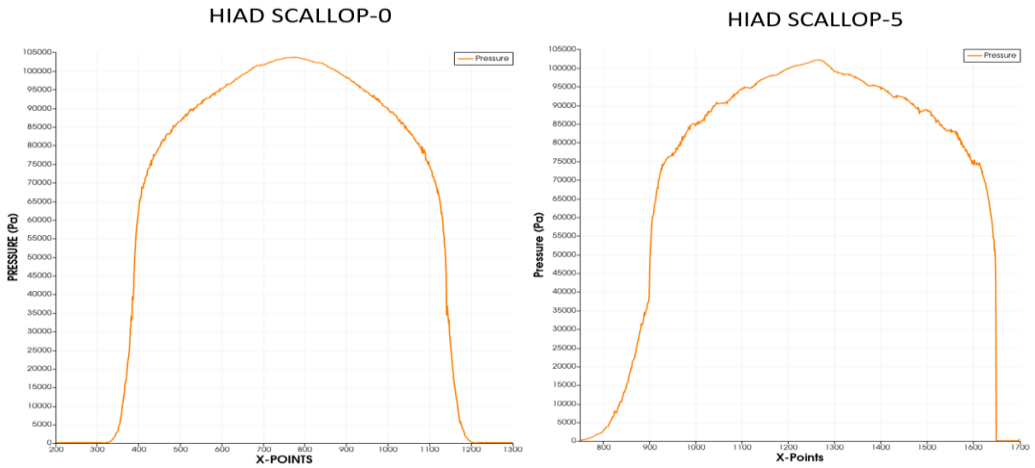

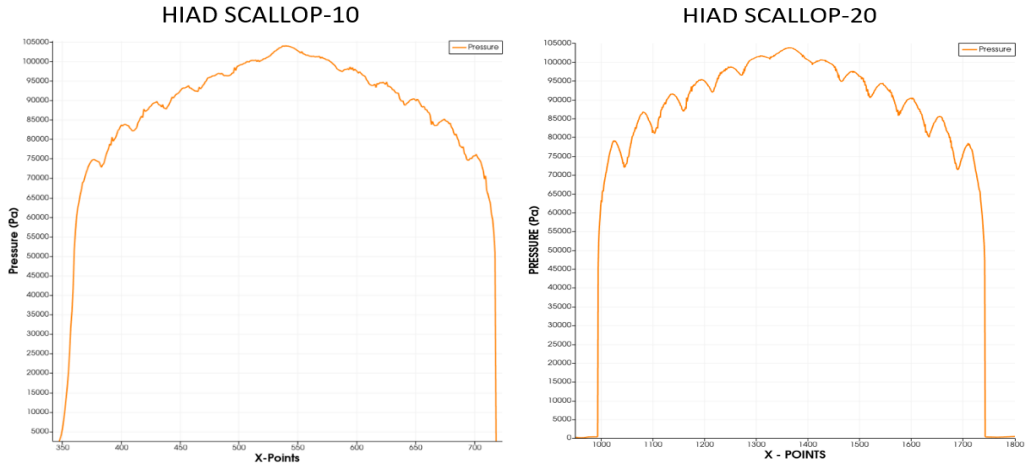

Figure 11 : Surface pressure for HIAD at various levels scalloping

Temperature contour comparisons of RANS and NEMO

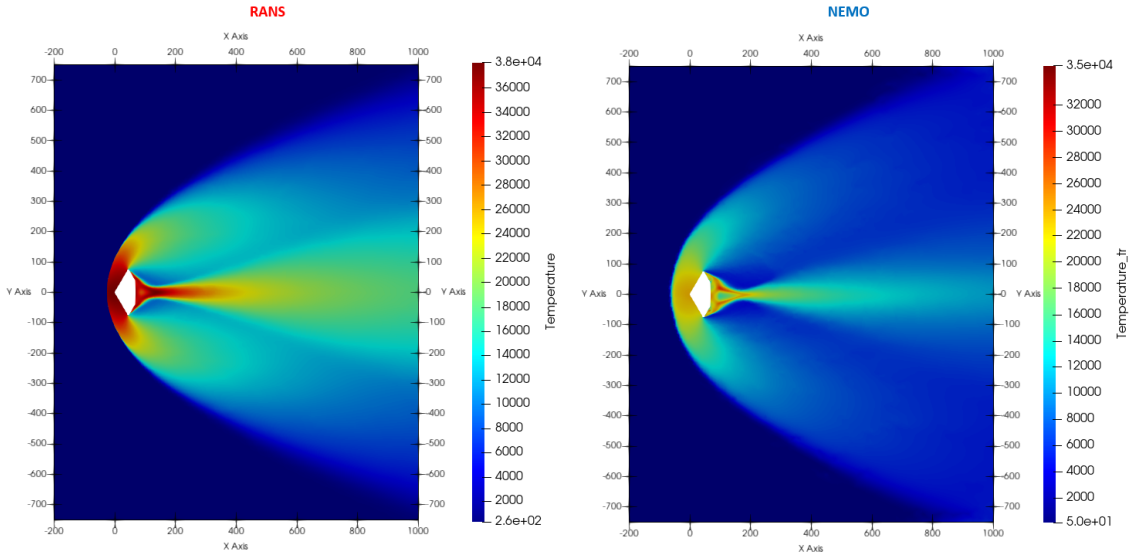

Figure 12 : RANS and NEMO temperature contours for HIAD-10

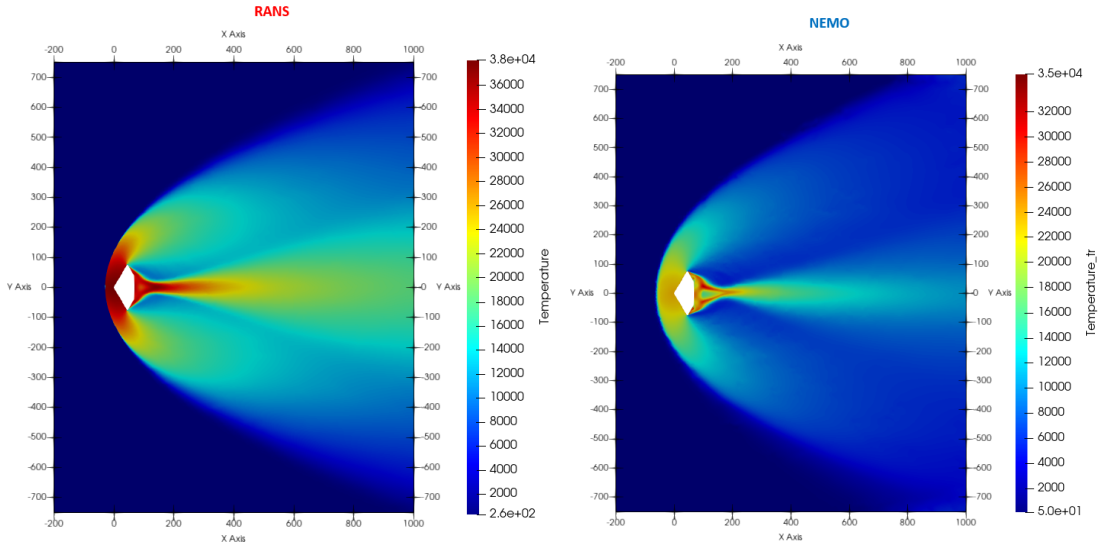

Figure 13 : RANS and NEMO temperature contours for HIAD-20

It can still be seen that the temperatures anticipated are significantly lower, leading to the conclusion that using a NEMO solver that considers non-equilibrium flow physics improves temperature prediction accuracy (see Figure 12 and 13). When considering non-equilibrium flow processes, the energy is all quantized into levels according to quantum mechanics. Due to molecular collisions at the tremendous temperatures faced by gas molecules during re-entry, vibrational and chemical changes occur. However, because of the low collision frequency of molecules at high altitudes, a significant number of collisions are required for the modifications to occur, which takes time.

This is why, in RANS simulations, temperature is estimated as a single energy state, i.e., the energy state in which molecules may only transfer energy by molecular excitation in translational directions, also known as translational energy. In the NEMO scenario, chemical processes that cause dissociation and recombination of molecules are examined together with vibrational, rotational, and electronic energy states. As a consequence, temperature estimations are greatly improved since the energy spent to dissolve molecules during the flow is taken into consideration. The substantially improved values of temperatures in the NEMO temperature contours demonstrate this.

5. Conclusions

The results from the present simulations conducted for the earth's atmosphere, were validated with NASA's experimental data. A similar set of simulations can be done for Martian atmosphere because the main purpose of developing HIAD was for planets with low density atmospheres. In the present work, chemically non-reacting flows were compared with chemically reacting non-equilibrium flows. This comparison was achieved by running simulations using the RANS solver and NEMO solver from which it was established that the ideal gas model over predicts temperatures while the NEMO solver using Mutation++ predicts the temperatures much more accurately as well as giving a much more realistic representation of the temperature contour.

In reality, atmospheric entry occurs at an angle of attack of approximately 15-20 degrees. Therefore, in the future, 3D-geometry and grid can be generated to study the effects of hypersonic flows over the module at various angles of attack.

References

1. Hollis, B.R., (2018) "*Surface heating and boundary-layer transition on a hypersonic inflatable aerodynamic decelerator*". *Journal of Spacecraft and Rockets*, 55(4), 2018.
2. Hughes, S., Cheatwood, F., Dillman, R., Calomino, A., Wright, H., DelCorso, J. and Calomino, A., (2011) "*Hypersonic inflatable aerodynamic decelerator (HIAD) technology development overview*". 21st AIAA Aerodynamic Decelerator Systems Technology Conference and Seminar (p.2524), 2011.
3. Calomino, Anthony, (2013) "*NASA HIAD Generation 1 Flexible Thermal Protection System Development and Flight Performance*", 22nd AIAA Aerodynamic Decelerator Systems Conference, Daytona Beach, FL March 25-28, 2013.
4. Cassell, Alan, (2013) "*Design and Execution of the Hypersonic Inflatable Aerodynamic Decelerator Large-Article Wind Tunnel Experiment*", 22nd AIAA Aerodynamic Decelerator Systems Conference, Daytona Beach, FL March 25-28, 2013.

5. Yates, J.T.; Johnson, J.K. (2007) "*Molecular Physical Chemistry for Engineers*", 1st ed.; University Science Books: Sausalito, CA, USA, 2007.
6. Anderson, J. D. (2004). "*Modern compressible flow*", McGraw-Hill, Singapore
7. Jeng, M., (2017). "*Aerothermodynamics and TPS Sizing of Skip Re-Entry and Aerocapture Vehicles*", Doctoral dissertation, San Jose State University, 2017.
8. Takahashi, Y. and Yamada, K., (2018). "*Aerodynamic heating of inflatable aeroshell in orbital reentry*". Acta astronautica, 152, pp.437-448, 2018.
9. Herdrich, G., Fertig, M. and Löhle, S., (2009). "*Experimental simulation of high enthalpy planetary entries*". *The Open Plasma Physics Journal*, 2(1), 2009
10. Morris, J. D., (1992) "*Convective Heat Transfer in Radially Rotating Ducts*," *Proceedings of the Annual Heat Transfer Conference*, edited by B. Corbell, Vol. 1, Inst. of Mechanical Engineering, New York, 1992, pp. 227–234.